Solid-State Conduction

DOI: 10.1002/anie.201003917

Mesoscopic Charge Carriers Chemistry in Nanocrystalline $SrTiO_3$**

Piero Lupetin, Giuliano Gregori, and Joachim Maier*

For a given compound, the deviation from the exact stoichiometry is the crucial chemical control parameter. Even if such deviations are small, they are of first order for the charge-carrier concentrations. This means that it is the oxygen nonstoichiometry in oxides that may determine whether a given oxide is n- or p-type, ionically or electronically conducting, or even superconducting. This nonstoichiometry, which is paramount for applications such as superconducting devices, fuel cell electrodes, solid electrolytes, or dielectrics, to name only a few examples, can be tuned by variation of the oxygen partial pressure under equilibrium conditions. Here, we report the striking result that the transition from macroscopic to mesoscopic nanocrystalline $SrTiO_3$, that is, a sheer size effect, is equivalent to a variation in oxygen partial pressure by as much as 12 orders of magnitude. In addition to the opposing variation of n and p conductivity by 3 orders of magnitude, the oxygen vacancy conductivity is depressed by 6 orders of magnitude.

These results can be all explained in the framework of the core–space charge concept. The basis for this is delivered by the field of nano-ionics,[1,2] which allows for the elucidation of defect chemistry not only for well-separated boundary zones but also in the more exciting mesoscopic range where the distance of the interfaces (grain size) is on the order or below the characteristic decay length of a semi-infinite interfacial zone.[3,4] In such cases, there is no unperturbed bulk.

There are various reports on the model material $SrTiO_3$, which show that boundary zones in ceramic material are typically Mott–Schottky layers (characterized by the Mott–Schottky length λ^*) resulting from a positive excess grain boundary (GB) core charge. This can be attributed to an inherent oxygen ion deficiency in the grain boundary core structure[5] and/or the segregation of dopant cations to interstices therein.[6,7]

Previous reports confirm depression of hole and vacancy conductivity at such boundaries and suggest increased excess electron contributions.[8–12]

$SrTiO_3$, a perovskite of great technological relevance, is also an excellent model material for functional ceramics because of its pronounced stability and its well-explored defect chemistry.[13–17] Balaya et al. recently showed that the bulk response in pure $SrTiO_3$ (with acceptor impurities concentration equal to 0.025 at.%) disappears when the average grain size is about 80 nm.[18–20] Here, we succeeded in preparing similar ceramics of even smaller grain size. Subsequent annealing allows for grain-size variation under defined conditions. Moreover, the samples allow us for the first time to study the stoichiometry dependence of the charge-carrier chemistry under mesoscopic conditions. The study of the overall conductivity as a function of oxygen partial pressure (P) reveals striking effects on the partial electronic and ionic conductivities and in particular on the n–p transition. All of them can be well interpreted, making this example not only the oxide counterpart of the CaF_2–BaF_2 heterolayers;[21] this $SrTiO_3$ master example is even more general (also compared to CeO_2)[22,23] as it highlights the mesoscopic effect on all three ionic, p-type, and n-type conductivities.

$SrTiO_3$ nanopowders were synthesized as described in Ref. [19] and sintered by using the high-pressure spark plasma sintering technique, which allowed us to obtain pellets with a grain size between 50 nm (Figure 1a) and 80 nm (Figure 1b). As can be seen in the inset of Figure 1b, because of the presence of intragranular porosity, the boundary spacing and,

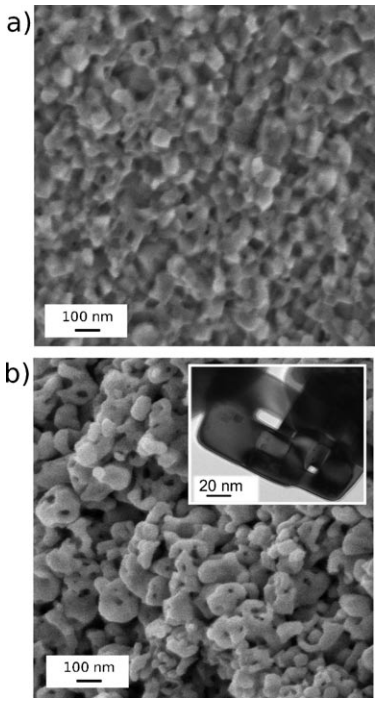

Figure 1. SEM micrographs of a) nanocrystalline dense $SrTiO_3$ and b) nanocrystalline $SrTiO_3$ with residual intragranular porosity. The TEM micrograph in the inset illustrates the presence of nanosized pores.

[*] P. Lupetin, Dr. G. Gregori, Prof. J. Maier
Max Planck Institute for Solid State Research
Heisenbergstrasse 1, 70569 Stuttgart (Germany)
E-mail: g.gregori@fkf.mpg.de

[**] We thank Prof. Palami Balaya for useful discussion and S. Kühnemann for SEM analysis. U. Salzberger and B. Rahmati are thanked for the TEM sample preparation and TEM analysis, respectively. A. Meyer and G. Werner are thanked for the chemical analysis of the samples.

Supporting information for this article is available on the WWW under http://dx.doi.org/10.1002/anie.201003917.

hence, the effective average grain size in the second sample is clearly lower, namely in the range of 30 nm. All these samples are found to contain ca. 10^{-2} at. % of acceptors (ca. 0.02 at. % according to the chemical analysis and ca. 0.01 at %. according to the conductivity measurements, see also the Supporting Information). For such an impurity content, $2\lambda^*$ exceeds the average grain size (for 0.02 at. % acceptor concentration, $\lambda^* \approx 50$ nm at 544 °C), λ^* being the Mott–Schottky space charge layer width.

Impedance spectroscopy was performed on all these samples at different temperatures as a function of P. Figure 2 gives representative spectra of the nanocrystalline material with the smallest effective grain size as well as the subsequently coarsened (microcrystalline) ceramic.

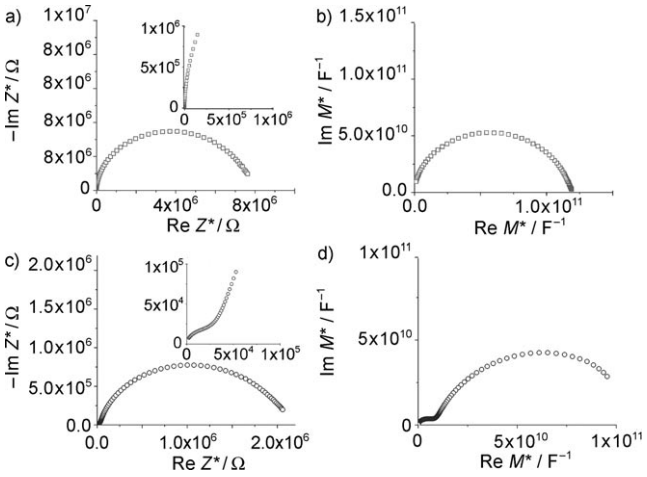

Figure 2. Impedance (Z^*) and modulus (M^*) spectra acquired at 544 °C and $P = 10^{-5}$ bar of the $SrTiO_3$ sample with effective grain size 30 nm. a) and b) refer to the nanocrystalline material, c) and d) refer to the coarsened sample. Note that the bulk contribution can be clearly recognized in (c) and (d), while (a) and (b) are characterized by one single semicircle.

While the nanocrystalline material for which the grain size is smaller than $2\lambda^*$ is characterized by a single semicircle (Figure 2a), a bulk arc in addition to the grain boundary signal can be observed in the microcrystalline material (Figure 2c). In the dielectric modulus plot, the high frequency contributions appear on the right hand side of the spectrum and can be easily resolved. The dielectric modulus spectrum for the nanocrystalline sample depicted in Figure 2b (one semicircle) indicates that the absence of a second semicircle at high frequency in the Z^* spectrum is not due to a poor resolution in the high frequency range but rather to the fact that there is no separate bulk contribution in the nanocrystalline material. This feature is an unambiguous argument only in the depletion mode, because in the accumulation mode, the bulk is short-circuited. Indeed, the bulk contributions for the microcrystalline sample are only detected in the regime of sufficiently high P (see also Figure S1 in the Supporting Information).

The activation energies determined for the nanostructured pellets in pure oxygen are 1.20 eV for the sample with grain size 50 nm and 1.45 eV for the sample with the smallest effective grain size, while being 0.8 eV (1.53 eV) for the bulk (GB) of the coarsened sample. These values are consistent with previous studies on $SrTiO_3$.[9,18]

Figure 3 shows the oxygen partial pressure P isotherms. The green line is obtained for an acceptor concentration of 0.01 at. % at 544 °C using the well-known bulk defect chemistry and mobility data for the charge carriers of $SrTiO_3$.[9] This curve describes very well the experimental data of the bulk of the coarsened sample (red open squares), as discussed below. The green line can be deconvoluted into an electronic conductivity itself (separately shown by the green dashed line) and a constant ionic conductivity σ_v, which is naturally particularly well seen around the minimum. The electronic conductivity is composed of an n-type branch (σ_n) that is only seen at very low P and a p-type branch (σ_p) with a transition occurring at 10^{-16} bar. When the partial pressure is increased, then—in the n-type regime—the incorporated oxygen increasingly consumes conduction electrons (oxidation of Ti^{3+} to Ti^{4+}). At higher P, the p-type conductivity dominates, which steeply increases with increasing P as the incorporated oxygen generates holes (oxidation of O^{2-} to O^-). (These chemical interpretations are of course not exact owing to the substantial orbital hybridizations.)

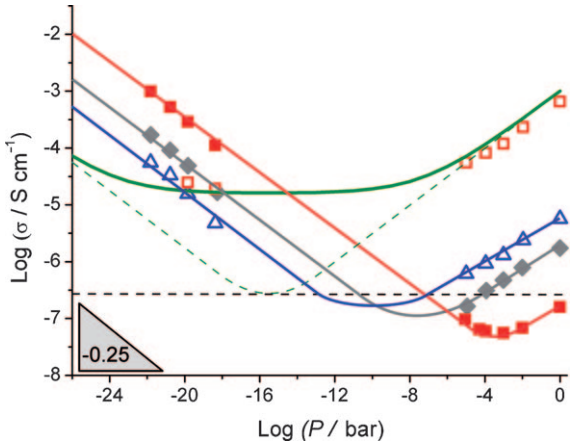

Figure 3. Conductivity versus oxygen partial pressure P measured at 544 °C. The symbols are assigned as follows: red open squares refer to the bulk of the microcrystalline $SrTiO_3$ obtained by coarsening the porous nanocrystalline sample; blue open triangles to the grain boundaries of the microcrystalline $SrTiO_3$; gray diamonds to nano $SrTiO_3$ 50 nm; solid red squares to nano $SrTiO_3$ with the effective grain size of ca. 30 nm. The green line illustrates the conductivity behavior of the microcrystalline bulk calculated according to the well-known defect chemistry of $SrTiO_3$ for $m = 0.01$ at. % according to Ref. [9]. The green dashed line shows the purely electronic conductivity and hence the conductivity minimum. The horizontal line represents the sum of p- and n-type conductivity at P_{min} corresponding to $2F\sqrt{u_n u_p K_B}$.

Notably σ_p and σ_n are coupled by the band–band mass action law $K_B = pn$ (K_B = corresponding equilibrium constant; p = hole concentration; n = excess electron concentration). For the p range, it suffices to formulate the oxygen incorporation process, which is given by $K_0 = p^2/(v P^{1/2})$ ($v =$

vacancy concentration). As the variation of v with P is tiny compared to the bulk concentration, which is fixed by the acceptor level ($\approx m/2$, m = acceptor concentration), the ion conductivity is practically constant. It then follows that $\sigma_n \propto P^{-1/4}$ and $\sigma_p \propto P^{+1/4}$.[24] These are well-established features for acceptor-doped alkaline earth titanates.[25–27]

The partial pressure at which the transition between p- and n-type conductivity occurs, is given by Equation (1) (see also the Supporting Information).

$$P_{min}(L \to \infty) = \left(\frac{K_B}{K_0}\right)^2 \frac{1}{v^2} \left(\frac{u_n}{u_p}\right)^2 = \left(\frac{K_B}{K_0}\right)^2 \frac{4}{m^2} \left(\frac{u_n}{u_p}\right)^2 \quad (1)$$

At P_{min}, both n- and p-type conductivity assume the same value given by $F\sqrt{u_n u_p K_B}$, F being the Faraday constant and u_n and u_p the mobility of electrons and holes, respectively. This simple expression (following directly from $p\,n = K_B$, $\sigma_p = \sigma_n$ at the minimum and from the definition of conductivity) is independent of the impurity content and it is valid also in the fully mesoscopic range, as we will see below.

The microcrystalline sample obtained by coarsening the nanosized porous sample exhibits a very similar isotherm if compared to the green literature curve.

The most remarkable results are exhibited by the nanocrystalline sample with the smallest effective grain size: compared with the coarsened sample, σ_p is depressed by more than 3 orders of magnitude while the n-type conductivity is enhanced by 2 orders of magnitude. The absence of any flattening (the narrow smooth region around the minimum is due to summing σ_n and σ_p) in the nanocrystalline curves means that the ionic (vacancy) conductivity is depressed by at least 3 orders of magnitude. Most striking is the giant shift of the minimum towards higher partial pressures (by 12 orders of magnitude). All these features including this enormous shift of the minimum by 12 decades are a consequence of the grain-size reduction and can be explained by the mesoscopic core–space charge model described below.

Compared to the bulk, the behavior in the space charge zone is completely different. All the carrier concentrations have to follow the space charge potential resulting from the core charge. As the core charge is positive, $p(x)$ is depressed by a factor $\kappa(x)$ (with $\kappa(x) = \exp[e\Delta\varphi(x)/RT]$; e = elementary charge, $\Delta\varphi$ = space charge potential), $n(x)$ is enhanced by the same factor, while $v(x)$ is depressed even by $\kappa(x)^2$ (owing to the double charge).[28] Figure 4 illustrates this situation. A precise interpretation has to calculate the effective resistances and conductances from the profiles and then to superimpose the contributions according to the distribution topology of the grains. This is, however, an almost impossible task. Fortunately, as we are in the mesoscopic regime, we can adopt the approximation of flat profiles. Under this assumption, the behavior is isotropic again and the equations shown above can be used by replacing the bulk concentrations with the concentrations directly adjacent to the core (i.e. at $x = 0$, designated with the lower index 0 and $\kappa_0 = \exp(e\Delta\varphi_0/RT)$).[29]

The latter is justified since we know from the literature[30] that the standard chemical potentials and, hence, the mass action constants are not perceptibly different from the bulk ones unless one approaches Angstrøm dimensions.

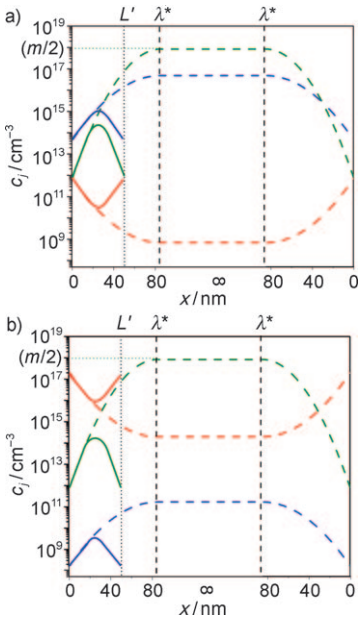

Figure 4. Calculated charge carrier profiles a) in pure oxygen and b) for $P = 10^{-22}$ bar for the 0.01 at.% acceptor doped sample at $T = 544\,°C$ and $\Delta\varphi_0 = 0.5$ V. Here the potential is assumed to be constant with grain size, although this may be only approximately correct, for example, Ref. [18]. The colors are assigned as follows: blue to holes, green to vacancies, and red to electrons. The dashed lines correspond to the coarsened sample $L > \lambda^*$ while the solid lines represent the profiles when $L < \lambda^*$ (nanocrystalline sample, which never reaches the bulk conditions).

At high P, the power laws of the nanocrystalline samples are 0.20 and thus lower than the value of the microcrystalline bulk (0.22)[24] indicating that $\Delta\varphi_0$ is slightly P dependent.[31,32] Notably, according to Equation (2) (whose derivation is included in the Supporting Information) κ_0 and therefore $\Delta\varphi_0$ can be determined from the ratio of P_{min} (nanocrystalline vs. bulk) yielding a value of 0.53 V for the nanocrystalline sample (30 nm effective grain size). This value is quite typical for $SrTiO_3$ ceramics and smaller than for the GB contribution in the coarsened sample (0.68 V, determined through Eq. S7).

$$P_{min}(L \to 0) = \kappa_0^4 P_{min}(L \to \infty) \quad (2)$$

A further point of interest is the following: despite the huge variations of $\sigma_n(P)$ and $\sigma_p(P)$ on size reduction, the minimum conductivities should stay invariant (owing to the assumption $K_{B,\infty} = K_{B,0}$) as long as the temperature remains the same. This follows from $\sigma_n = Fu_n n_0 = Fu_p p_0$ and $K_{B,0} = n_0 p_0$. This striking invariance, not only as far as size variation is concerned but also with respect to the impurity content, is approximately confirmed by Figure 3.

As already mentioned, this down-sizing effect is reversible as by coarsening we return to the bulk defect chemistry (red open symbols in Figure 3). Annihilation of grain boundaries leads to a homogenization of the charge-carrier separation.

Now, let us consider the asymmetric depression (enhancement) of σ_p (σ_n) of the nanocrystalline sample: compared with the coarsened sample, σ_p is depressed by more than 3 orders of magnitude whereas the n-type conductivity is enhanced by

2 orders of magnitude. Notably, this behavior is also observed for the GB conductivity of the coarsened sample (blue triangles in Figure 3) and this indicates that also size effects such as variation of mass action constants due to electron-confinement can be excluded (also the anisotropy of the electronic transport paths can be discarded as explanation). Hence, we rather ascribe this to a decrease of $\Delta\varphi_0$ with decreasing P. A more detailed analysis will be given in a forthcoming paper.[33]

Further information on the value of $\Delta\varphi_0$ comes from the comparison of the activation energies for bulk and GB (see also Eq. S9). The difference of 0.72 eV is comparable with the results reported in Ref. [18] and contains $\Delta\varphi_0$ as well as its temperature dependence. Adopting the temperature dependence for the GB of the coarsened sample (0.12 eV, obtained using $\Delta\varphi_0 = 0.68$ V of the coarsened sample in Eq. S9) we are left with 0.6 eV, which is close to the above 0.53 eV. The remaining difference can be easily explained as an artifact of the flat profile assumption.

These considerations nicely explain also the different behavior of the nanocrystalline sample with slightly larger grain size (50 nm). As shown in Figure 3 (gray diamond symbols), for this sample the shift of P_{min} is still very large but less pronounced (8 orders of magnitude instead of 12) than in the sample with the smallest effective grain size. Also σ_p is less depressed (2.5 orders of magnitude) while σ_n is enhanced only by half an order of magnitude.

In summary, we reported on the conductivity of nanocrystalline $SrTiO_3$ as a function of oxygen partial pressure and compared it with the properties of the coarsened material. The isotherms unfold the full mesoscopic defect chemistry with greatly modified n-, p-, and oxygen vacancy-type conduction. It is remarkable how well these significant variations and in particular the shift of the p–n transition partial pressure by as many as 12 orders of magnitude can be understood in terms of the generalized ionic–electronic space charge model. The results make nanocrystalline $SrTiO_3$ a most impressive master example of defect chemistry in the nanoregime and demonstrate the enormous power of size as degree of freedom in modern materials research.

Experimental Section

$SrTiO_3$ powders were synthesized according to the method described in Ref. [19]. In the case of the porous samples, iron nitrate hydrate was added into the titanium solution, before the reaction with strontium nitrate took place. X-ray patterns (XRD) confirmed that all the powders consisted of a single phase. The grain size calculated by Brunauer–Emmett–Teller (BET) method was about 30 nm for the dense $SrTiO_3$ powder and 50 nm for the powder with intragranular closed porosity. In order to obtain dense nanocrystalline materials, the powders were sintered using a spark plasma sintering (SPS) press (HP D 5, FCT Systems GmbH). The commercial setup was modified similarly to what reported in Ref. [34]. The $SrTiO_3$ samples were sintered at 850 °C for 5 min applying a pressure of 400MPa. The density, determined by the Archimedes' method, were above 90 % for all samples. In order to compare the conduction properties between nano- and microcrystalline samples, a porous pellet was annealed in air at 1250 °C for 4 h after SPS sintering. Its average grain size was about 1 μm.

Impedance spectroscopy measurements were performed (with sputtered platinum electrodes) using an Alpha-A high resolution dielectric analyzer (Novocontrol) (ac voltage 0.3 V, frequency range from 1 MHz to 1 Hz). The samples were first equilibrated in the desired P range (ranging between 10^{-5} and 1 bar and, using $CO–CO_2$ mixtures, between 10^{-19} and 10^{-22} bar) at 550 °C for 20 h and then investigated between 550 and 450 °C at intervals of 10 °C.

Received: June 28, 2010
Revised: September 8, 2010
Published online: November 29, 2010

Keywords: charge transport · conductivity · mesoscopic effect · perovskites · solid-state chemistry

[1] J. Maier, *Nat. Mater.* **2005**, *4*, 805.
[2] J. Maier, *Phys. Chem. Chem. Phys.* **2009**, *11*, 3011.
[3] J. Maier, *Solid State Ionics* **2002**, *148*, 367.
[4] H. L. Tuller, *Solid State Ionics* **2000**, *131*, 143.
[5] C. L. Jia, K. Urban, *Science* **2004**, *303*, 2004.
[6] H. Avila-Paredes, S. Kim, *Solid State Ionics* **2006**, *177*, 3075.
[7] G. Gregori, B. Rahmati, W. Sigle, P. van Aken, J. Maier, *Solid State Ionics* **2010**, DOI: 10.1016/j.ssi.2010.07.020.
[8] R. Waser, *J. Am. Ceram. Soc.* **1991**, *74*, 1934.
[9] I. Denk, J. Claus, J. Maier, *J. Electrochem. Soc.* **1997**, *144*, 3526.
[10] P. C. McIntyre, *J. Am. Ceram. Soc.* **2000**, *83*, 1129.
[11] X. Guo, J. Fleig, J. Maier, *Solid State Ionics* **2002**, *154–155*, 563.
[12] C. Ohly, S. Hoffmann-Eifert, X. Guo, J. Schubert, R. Waser, *J. Am. Ceram. Soc.* **2006**, *89*, 2845.
[13] R. Hagenbeck, R. Waser, *J. Appl. Phys.* **1998**, *83*, 2083.
[14] R. Moos, K. H. Härdtl, *J. Am. Ceram. Soc.* **1997**, *80*, 2549.
[15] G. E. Pike, C. H. Seager, *J. Appl. Phys.* **1979**, *50*, 3414.
[16] R. A. De Souza, J. Fleig, R. Merkle, J. Maier, *Z. Metallkd.* **2003**, *94*, 218.
[17] R. A. De Souza, J. Fleig, J. Maier, O. Kienzle, Z. Zhang, W. Sigle, M. Rühle, *J. Am. Ceram. Soc.* **2003**, *86*, 922.
[18] P. Balaya, J. Jamnik, J. Fleig, J. Maier, *Appl. Phys. Lett.* **2006**, *88*, 062109.
[19] P. Balaya, M. Ahrens, L. Kienzle, J. Maier, B. Rahmati, S. B. Lee, W. Sigle, *J. Am. Ceram. Soc.* **2006**, *89*, 2804.
[20] P. Balaya, J. Jamnik, J. Fleig, J. Maier, *J. Electrochem. Soc.* **2007**, *154*, P69.
[21] N. Sata, K. Eberman, K. Eberl, J. Maier, *Nature* **2000**, *408*, 946.
[22] S. Kim, J. Maier, *J. Electrochem. Soc.* **2001**, *149*, J73.
[23] A. Tschöpe, R. Birringer, *J. Electroceram.* **2001**, *7*, 169.
[24] It is worth to note here that if the material contains redox active acceptors a deviation of the P dependence from 1/4 to lower values is expected.
[25] See e.g.: J. Daniels, K. H. Härdtl, D. Hennings, R. Wernicke, *Philips Res. Rep.* **1976**, *31*, 487.
[26] N.-H. Chan, R. K. Sharma, D. M. Smyth, *J. EIectrochem. Soc.* **1981**, *128*, 1762.
[27] U. Balachandran, N. G. Eror, *J. Solid State Chem.* **1981**, *39*, 351.
[28] J. Maier, *Prog. Solid State Chem.* **1995**, *23*, 171.
[29] J. Maier, *Faraday Discuss.* **2007**, *134*, 51.
[30] E. A. Kotomin, V. E. Alexandrov, D. Gryaznov, R. A. Evarestov, J. Maier, *Phys. Chem. Chem. Phys.* **2010**, DOI: 10.1039/c0cp01060j.
[31] Z. Zhang, W. Sigle, R. A. De Souza, W. Kurtz, J. Maier, M. Rühle, *Acta Mater.* **2005**, *53*, 5007.
[32] R. A. De Souza, *Phys. Chem. Chem. Phys.* **2009**, *11*, 9939.
[33] G. Gregori, P. Lupetin, J. Maier, unpublished results.
[34] U. Anselmi-Tamburini, J. E. Garay, Z. A. Munir, *Scr. Mater.* **2006**, *54*, 823.

